Manufacturing and characterization of the sword "Berkelium"
The University of California, Berkeley Team

Students: Hi-Tin Vo[1], Nathan Bailey[1], David Frazer[1], Rachel Traylor[2], Rachel Connick[1], William Connick[3]

Artesian Advisor: James Austin[4]

Academic Advisor: Professor Peter Hosemann[1]

Technical Advisor: Jeff Bickel[1]

[1] University of California Berkeley, Department of Nuclear Engineering, Etcheverry Hall, 94720 Berkeley, CA

[2] University of California Berkeley, Department of Materials Science and Engineering, Hearst Mining Hall, 94720 Berkeley, CA

[3] University of California Berkeley, Department of Mechanical Engineering, Etcheverry Hall, 94720 Berkeley, CA

[4] Alchemy Metalworks 2440 Adeline, Oakland, CA

Forgings, experimentation, and metallurgical analyses were conducted by the UC Berkeley team with the oversight and advising of Jim Austin, Jeff Bickel and Peter Hosemann

1. Table of contents

2. Blade manufacturing process – from ore to sword

Details of the UC Berkeley blade manufacturing process are discussed in following section. All work was conducted in Mr. James Austin's forging shop in downtown Oakland CA. The shop is equipped with the proper tools and infrastructure to complete this project. Mr. Austin was the artisan advisor and supported the effort by guiding the team through the process of manufacturing the blade Berkelium. Jeff Bickel provided guidance in the safety matters while Prof. Peter Hosemann had the oversight of the project.

2.1. Ore Collection, separation and refining

The steel used for the blade was fabricated from raw materials, i.e. ore, which tremendously enhanced the educational experience generated by this project for the entire team. Since iron (Fe) has a strong affinity for oxygen (O), elemental Fe is generally found in the form of iron oxides, termed iron ores. These ores are also known to contain varying quantities of other elements such as silicon (Si), sulfur (S), manganese (Mn), and phosphorus (P). Magnetite (Fe_3O_4) is an iron ore that can be found around some public beaches in northern California [1]. The distribution of magnetite varied for different beaches and was especially abundant along strongly eroded areas as indicated in [1]. The magnetite content in the sand on the beaches is also dependent on the time of the year the raw materials is collected. This is most likely a consequence of the seasonal influence on erosion, i.e. the degree of erosion increases during times of heavier rainfall and wind currents [1]. Areas of magnetite were identified fairly easily due to its dark appearance of the sand as shown in Figure 1. Approximately five gallons of magnetite-containing sand were collected and brought back to the Alchemy Metallworks forging shop for further processing. The sand collected also contained hematite (Fe_2O_3), another common iron ore, as well as a large number of non-ferrous elements. Further filtering of the sand was critical before starting the Fe refinement process to minimize impurities in the steel, which ultimately enhanced the quality of the blade. Since magnetite has a higher iron-to-oxygen ratio than hematite and iron is naturally magnetic, the higher Fe content in magnetite is the fundamental reason why it is much more magnetic than hematite. This allowed for easy segregation of magnetite from the other elements and compounds in the sand via magnets as shown in Figure 1-a. It should be mentioned that the sand was spread thinly over a large cleaned area and neodymium magnets were carefully passed over the sand collecting magnetite. It was important to keep the magnet far enough away from the sand to prevent clumps of the magnetite-enriched sand from jumping onto the magnet since clumps were more likely to contain impurities. Approximately 50% of the sand collected from the beach was magnetic and therefore used for further processing. For clarity, the magnetic portion of the collected sand at this point will just be referred to as magnetite.

Charcoal was the primary carbon (C) source for the reduction of magnetite to pure iron. The charcoal was broken up into fine dust as it is shown in Figure 1-c. Ventilation masks were mandatory during this process as it generated a significant amount of dust. Calcium carbonate ($CaCO_3$) was mixed with the charcoal in order to help with removing silicon from the melt.

Figure 1: Filtering magnetite-enriched sand from the local northern California beach. (a) Spreading the sand on a cleaned flat surface; (b) carefully collecting magnetite from the sand with neodymium magnets in plastic cups; and (c) grinding the charcoal and mixing in the $CaCO_3$ for the smelting process.

2.2. Smelting the raw materials into steel

Smelting is the process by which the iron ore is reduced to iron. The smelting process for the UC Berkeley blade took place as follows. A homogeneous dry mixture consisting of 1200g (75%) magnetite, 200g (12.5%) crushed charcoal, i.e. carbon, 200g (12.5%) $CaCO_3$, and some mount of glass (SiO_2) was contained in a graphite/clay crucible and placed in a homemade natural gas fired rudimentary blast furnace insulated with refractory ceramic fibers (RCF), illustrated in Figure 2. The crucible was positioned near the center of the furnace setup for more even heating and sat on a stack of insulating firebrick (IFB). The graphite crucible was selected since it could withstand the intense temperatures necessary for smelting and also acted as a secondary carbon source for reduction process. Air was blasted into the bottom of the furnace using a high power fan coupled with the natural gas to intensify the combustion process and continually remove the gaseous byproducts, thereby allowing the necessary chemical reactions to continue for the duration of the smelt (approximately 1.5-3 hours). The consistency of the smelt was checked periodically with an iron rod. It was found that the material mixture in the crucible did not melt for 45 minutes to 1 hour. This was likely due to the fact that the reduction of magnetite to Fe is based on the fact that diffusion must take place. The carbon must reduce the Fe_3O_4 in the solid state since the melting point of magnetite cannot be reached in our furnace. Subsequently the ingot can only be liquefied if all the magnetite is reduced. Therefore checking to see if the ingot is liquid can tell us if the majority of the magnetite is reduced. In addition the increasing carbon content reduces the melting point according with the face diagram. Pure Fe has a melting point of 1539°C according to the phase diagram displayed in figure 3 while Fe with some amount of carbon as it was found to be the case here has a melting point below 1500°C.

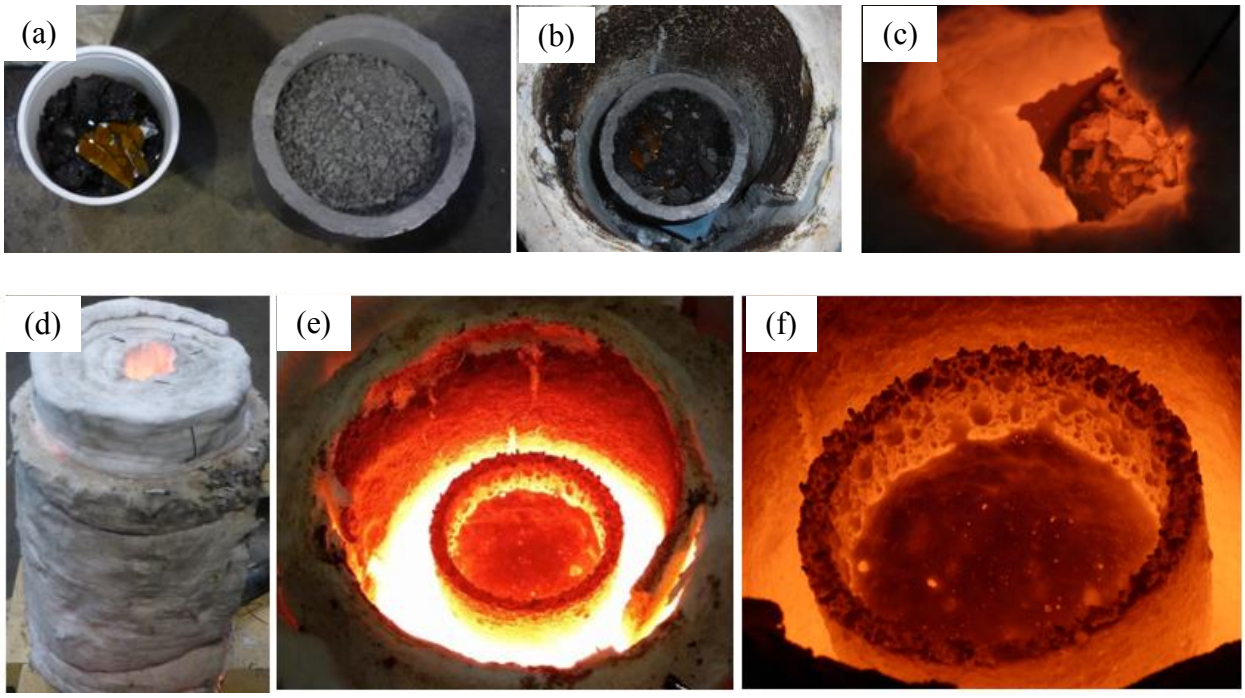

Figure 2: (a) (left) Crushed charcoal and glass in a plastic container, (right) magnetite after mixing with $CaCO_3$ and charcoal; (b) crucible and mixture inserted into the homemade furnace; (c) observation of the process during heat up; (d) the complete furnace setup, insulated with refractory ceramic fibers around the exterior to control heat dissipation; (e) the graphite crucible inside the furnace at the beginning of the cooling process; (f) close-up of the smelt during cooling after approximately one hour of cooling.

The actual chemical process ongoing during the smelting process is rather complicated however all likely carbon based reduction reactions for magnetite and hematite are explained in the following equations.

$$Fe_3O_4 + 4C \rightarrow 3Fe + 4CO \quad \text{Equation 1}$$
$$Fe_3O_4 + 4CO \rightarrow 3Fe + 4CO_2 \quad \text{Equation 2}$$
$$Fe_3O_4 + 2C \rightarrow 3Fe + 2CO_2 \quad \text{Equation 3}$$
$$Fe_3O_4 + CO \rightarrow 3FeO + CO_2 \quad \text{Equation 4}$$
$$FeO + CO \rightarrow Fe + CO_2 \quad \text{Equation 5}$$
$$3Fe_2O_3 + CO \rightarrow 2Fe_3O_4 + CO_2 \quad \text{Equation 6}$$
$$Fe_2O_3 + 3C \rightarrow 2Fe + 3CO \quad \text{Equation 7}$$
$$2Fe_2O_3 + 3C \rightarrow 4Fe + 3CO_2 \quad \text{Equation 8}$$
$$Fe_2O_3 + 3CO \rightarrow 2Fe + 3CO_2 \quad \text{Equation 9}$$

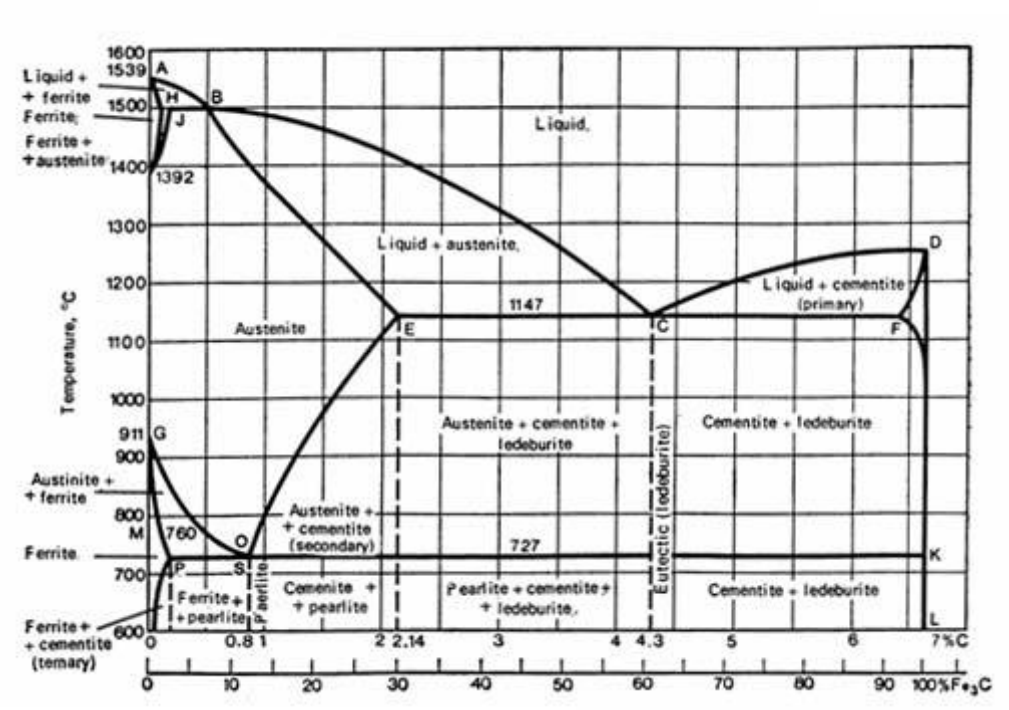

Figure 3: Iron-carbon binary phase diagram [2] (metastable)

The flux agents, $CaCO_3$ and glass (SiO_2), further reduced the amount of impurities accompanying the iron ore by reacting with the rock gangue to produce a glass-like byproduct, termed slag. The following equations illustrate some of the chemical reactions that can occur when purifying the smelt via slag formation.

$$CaCO_3 + SiO_2 \rightarrow CaSiO_3 + CO_2 \quad \text{Equation 10}$$

$$CaCO_3 \rightarrow CaO + CO_2 \quad \text{Equation 11}$$

$$CaO + SiO_2 \rightarrow CaSiO_3 \quad \text{Equation 12}$$

$$Si + O_2 \rightarrow SiO_2 \quad \text{Equation 13}$$

$$4P + 5O_2 \rightarrow P_4O_{10} \quad \text{Equation 14}$$

Slag is less dense than molten iron and floats to the top of the crucible, which protects the underlying molten Fe from the environment and re-oxidation. The density and viscosity of molten iron directly influence the amount of slag inclusions in the ingot. The hotter and longer the smelt, the better the reduction and separation of iron from the raw materials. However, the amount of time and heating power required for a complete separation are unreasonably high, forcing the team to balance ingot quality with time and production costs. Just before turning off the furnace aluminum (Al) was added in small quantities via an Al rod. This process is also known as "killing the steel". The Al serves as oxygen gather which captures the dissolved oxygen in the liquid metal during cooling and solidification, thereby reducing the overall porosity of the solid metal. After cooling, the disk shaped ingot was removed from the crucible, displayed in Figure 4. The result was a porous mass of an iron-carbon alloy and slag. It was found that 1200g magnetite formed 800g solid metal by this smelting process. Considering only the Fe and carbon one can conclude that 1200g magnetite which contains 73.3wt% Fe and 26.7wt% oxygen leads to 876g Fe and 324g

oxygen. One can further estimate assuming that the final carbon product is CO_2 only used 100g carbon suggesting that just below 100g carbon was lost during this process. The estimated 876g Fe estimated matches reasonable well with the measured 800g Fe per ingot.

Figure 4: High carbon as smelted ingot.

This smelting process was repeated five times in order to create approximately 4kg of steel. Two of the five ingots were manufactured with less carbon content. Both ingot-types had the same initial magnetite: carbon: calcium carbonate ratios, but differed in total smelting time. The smelt time for the lower carbon content ingots was shorter, thereby reducing the amount of carbon diffusion. The carbon content of each ingot was quantified via spark testing, outlined in [3,4]. The sparks produced on the material were compared to a chart, shown in Figure 5. Spark testing attempts to assess the carbon content by the shape of the sparks created during grinding of the steel. Under experienced supervision of the artesian team member it was found that the two different ingots indeed show different carbon content. An exact assessment of carbon was not made at this point and the ingots were only classified as high carbon and low carbon ingots.

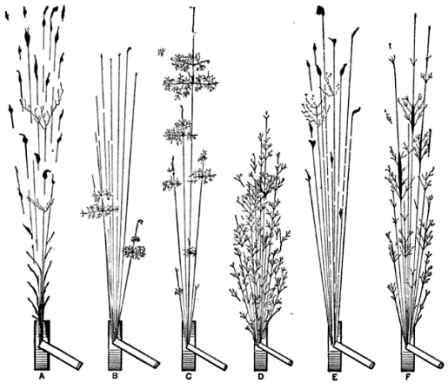

Figure 5: Spark testing chart [4] (A) Wrought iron (B) Mild steel (C) Steel with 0.5 to 0.85% carbon(D) High-carbon tool steel(E) High-speed steel(F) Manganese steel

2.3. Forging the steel into a sword

Each ingot was cut into three segments using a high-speed saw. The segments were heated to approximately 800°C for further processing. All fifteen segments were hand forged into thin strips by students in alternating teams of three. The repetitive hammering and heating helped drive out large slag inclusions and reduced porosity. Due to the intense labor required for hand forging, this step took several sessions to complete. Once formed, the hand-forged strips were shaped into equal rectangular strips with a power hammer operated by Mr. Austin. Due to safety concerns the use of the students of the power hammer was limited.

Figure 6: (a) A sponge iron ingot segmented into three strips; (b) and (c) hand forging the segments in (a) into thin strips; (d) resulting hand-forged strips from one session.

The strips were sand blasted and mechanically ground to remove large oxide pieces. Subsequently they were cut into three pieces and stacked on top of one another. One short edge of the stack was ground with a belt sander to flush the strips together. A long steel handle was welded to this flat edge for easier handling and the pieces were forge welding back together. The stack of 4 billets was the starting material for the lamination process, which was conducted as follows: The material was forge welded together by hand using Borax as a flux agent to prevent excessive oxidation during the process. The forging started on one of the billet and it was hammered along its length in order to drive out any pores which might be trapped in between. After initial forge welding the now thicker piece was evenly drawn out by heating and hammering while maintaining constant width. After the piece was drawn out the piece was cut again into 3 pieces and welded again onto a new handle in order to achieve another round of laminating leaving 12 folding. The low carbon pieces were again fold onto itself leaving now 36 folding on the low carbon material. Due to the fact that less high carbon material was amiable only 12 folding were conducted. During the forge welding process a fluxing agent, Borax ($Na_2(B_4O_7)$) was sprinkled all over the packets The resulting product, shown in Figure 7, was forged into shape with a power hammer. The predefined low carbon and high carbon metals were kept separate during this process.

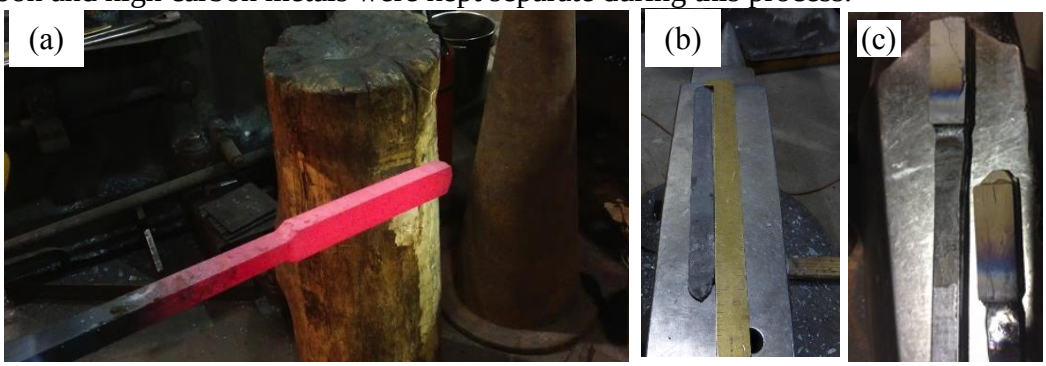

Figure 7: a) Billet package after forge welding b) drawn out ingot package c) and cut and re-welded billet for further laminating.

At the end of the strips were forged welded into three large packets, two low carbon (36 folding) and one high carbon (12) folding's, with the power hammer. These three packets were then forge welded together, again using the power hammer, with low carbon steel sandwiching the high carbon steel, as shown in Figure 8. The resulting unified metal was then ready to be shaped into a blade.

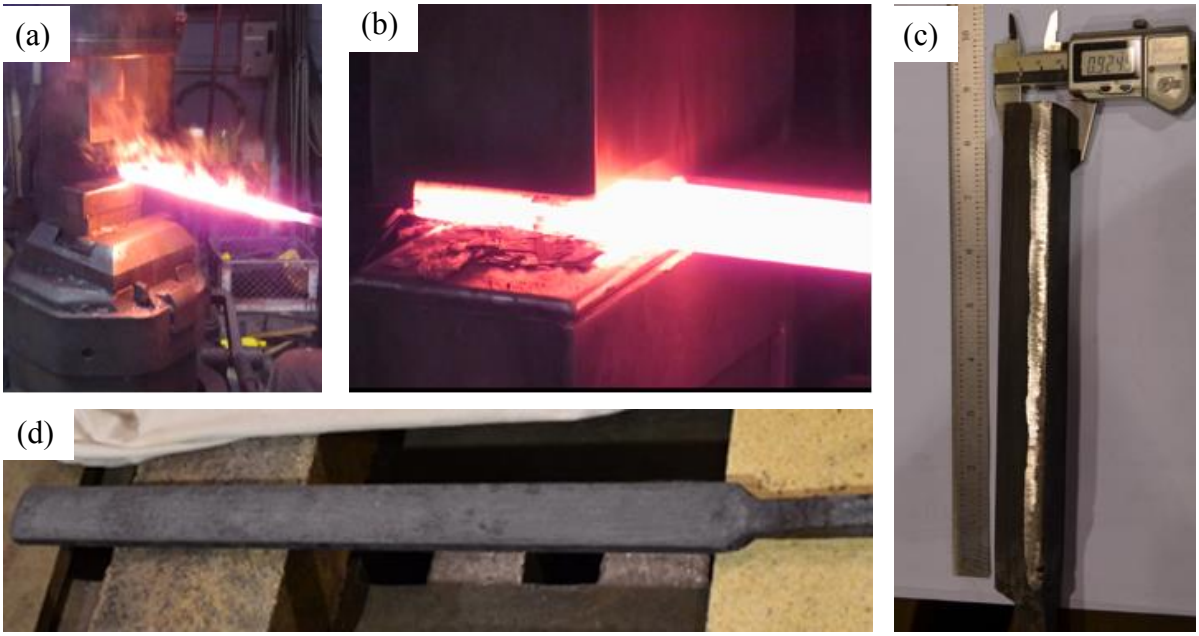

Figure 8: Laminating the low and the high carbon steel together and forge welding the strips using a power hammer.

The laminated and drawn out raw blade with a dimension of ~1.25" (~31.8mm) with and ~22" (558mm) length. The actual shape of the blade was decided by evaluating several different possible designs. The team found the design of a classical Sax blade was specifically appealing due to its simple but straight appearance. The actual forging of the shape was performed by hand. First the tip of the blade was formed by careful hitting the blade in an angle as shown in figure 9a. Continues straightening of the blade was necessary. For the actual edge of the blade a leveler tool was used with a striker in order to get an even angle on the blade to minimize subsequent grinding. Sectional reheating between processing steps were necessary while the blade had to be cleaned off with a wire brush in between in order to not incorporate too many oxide particles on the surface. The end piece, tang, was also formed by hand in a similar fashion utilizing the lever tool and a striker.

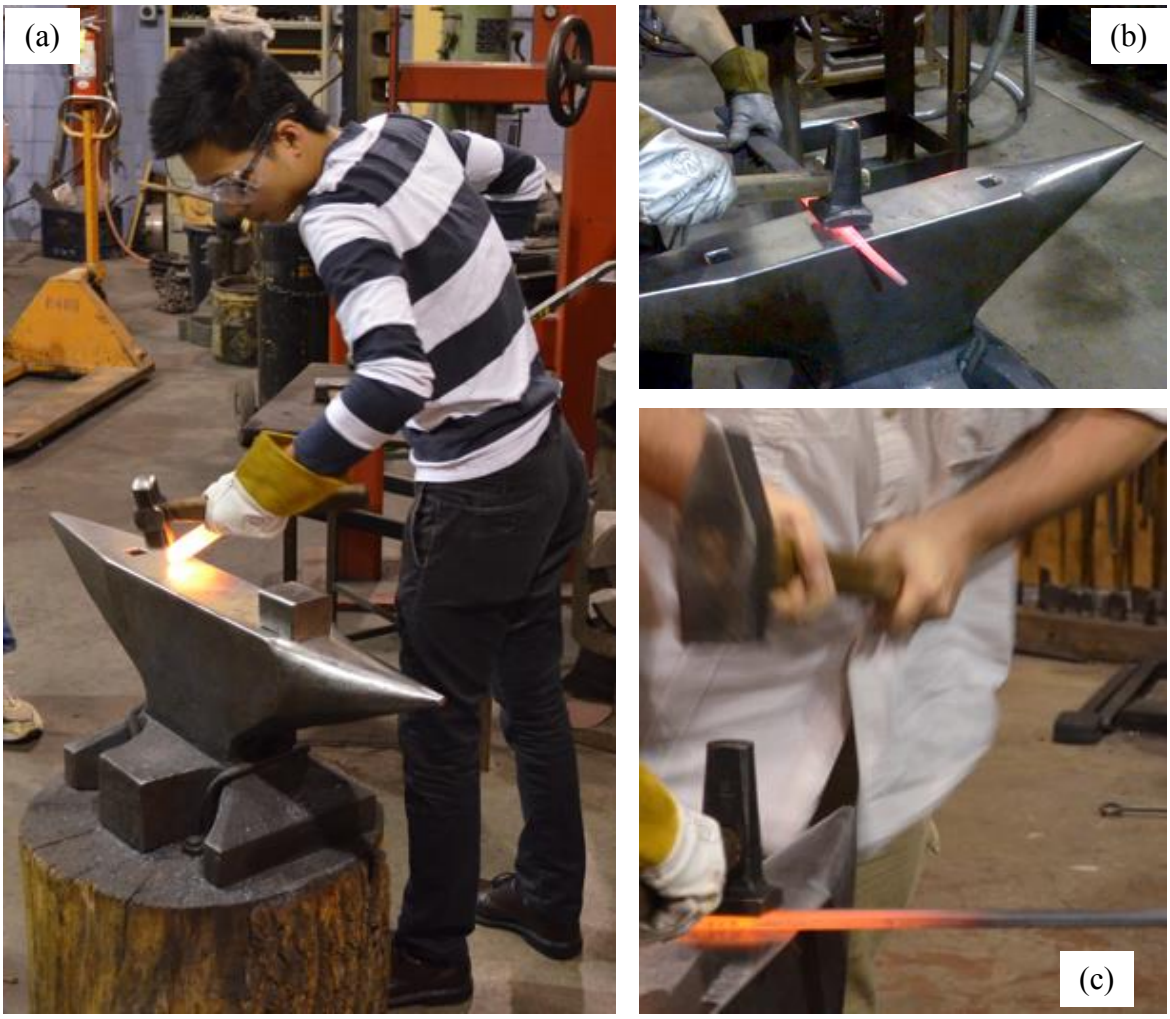

Figure 9: Forming the strip into a blade by Hand. (a) Forming the tip; (b) forming the handle's tang; (c) and forming the edge.

The as-forged blade had to be cleaned from surface oxides and ground into its final shape. A sand blaster was used for initial cleaning and the blade was shaped with a belt sander. This process is illustrated in Figure 10.

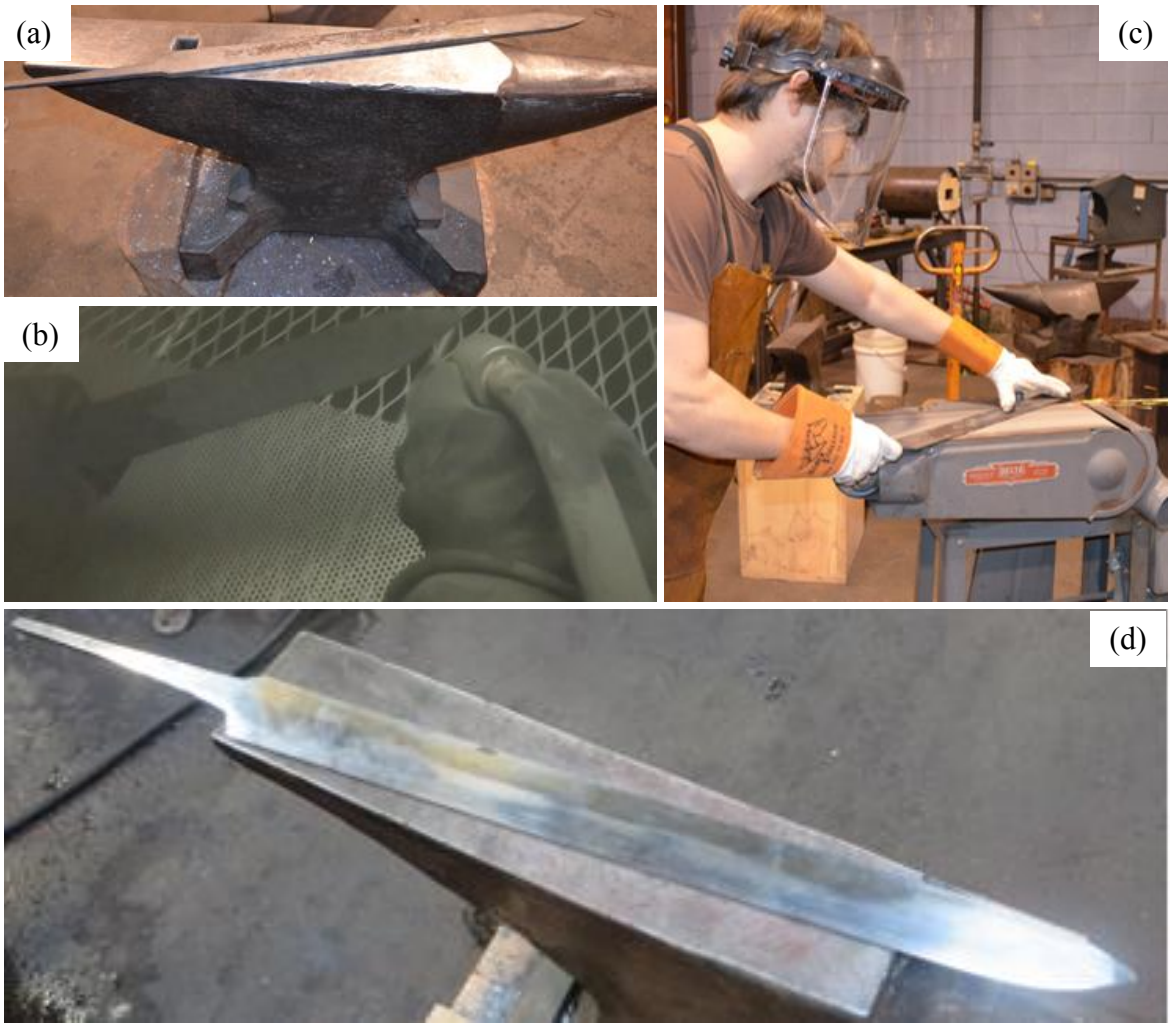

Figure 10: (a) Rough shaped blade; (b) sand blasting the as-forged blade; (c) grinding the blade on a belt sander; (d) and the rough ground blade.

2.4. Heat treating and hardening the sword

The blade was covered in a plaster mix of figure clay, grog (or previously fired clay), and cellulose fiber in order to control the quench rate. The purpose of doing this is to control the cooling rates on the edge and the body of the blade. Leaving the edge of the blade plaster free leads to a more dramatic cooling rate than the area which has been covered in plaster. This would allow to achieve a higher hardness in the edge area while the body of the blade was still more ductile and the blade is therefore less likely to break in a brittle fashion. The blade was than heated to 800°C (above the austentisation temperature) held for 15 minutes, and quenched in oil to room temperature. This treatment will allow to form martensite in the blade. Next it was tempered in a conventional oven at 200°C for one hour.

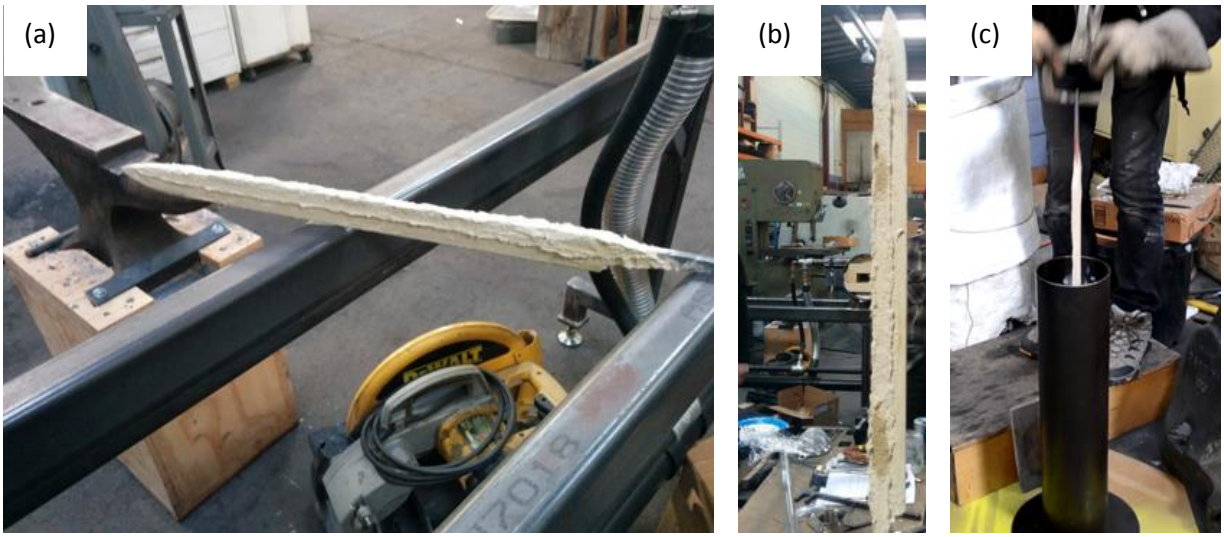

Figure 11: (a) and (b) Plaster coating prior to quench; and (c) quenching the blade in oil.

2.5. Final sword manufacturing steps

After hardening, the blade was polished with increasingly finer grades of silicon carbide papers by hand. Due to the length of the blade the use of the polishing machine was limited. The grits used were 320, 400, 600, 800 and 1200 followed by a final polishing on a soft cloth and 6um diamond paste. Next, the polished blade was slightly etched with Nital (3%nitric acid) etching solution to elucidate the laminating pattern indicative of forge welding as it can be seen in figure 12. The handle was manufactured out of stainless steel sheet metal. The shape of the cross pieces was cut out using a water jet cutter and fit to the blade. Before mounting the cross pieces to the blade the stainless steel was colored using the natural oxidation of the steel at elevated temperature. The golden color was achieved by oxidizing the stainless steel at 500°C for ~15 minutes until the desired color was achieved. The handle grip itself was made by wrapping a band around the tang area. This will ensure a solid grip when holding the blade. Images of the final blade are shown in Figure 12.

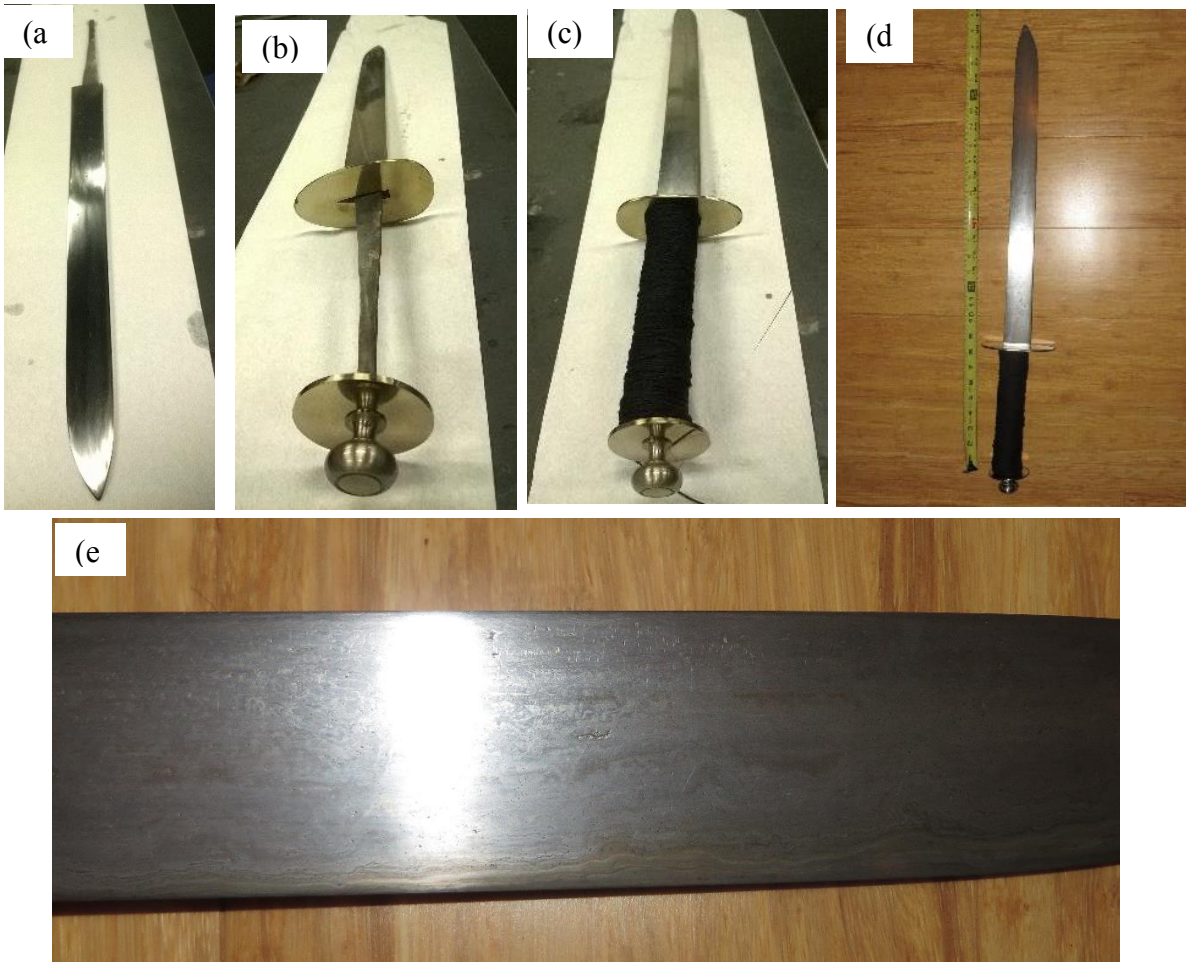

Figure 12: Images of the blade a) and the handle assembly process.(b-d). Photograph of the final blade as it is etched.

3. Metallurgical analysis of the blade

Multiple experiments were performed on the UC Berkeley sword and on pieces of a 1000-year-old spearhead donated to us by the artesian member of the team which was purchased in an auction to evaluate and directly compare the materials' properties.

3.1. Experimental

3.1.1. Equipment and methods

The hardness of the metals was measured during several stages of the sword manufacturing process using the Vickers hardness testing method. Optical Microscopy (OM) with a Zeiss Optical Microscope and maximum magnification of 1000x was conducted to examine the metal surface features both before and after etching. An FEI Quanta 3D dual-beam scanning electron microscope (SEM) and focused-ion beam (FIB) equipped with energy dispersive X-ray spectroscopy (EDS) capabilities was used for high-quality surface imaging coupled with elemental mapping to identify the compositions of the inclusions.

3.1.2. Materials examined

1. Samples of both the low carbon as-smelted ingots were extracted for an initial microstructure analysis.
2. Samples of both the low and high carbon laminated steel, prior to forge welding into a single billet, were evaluated to document any microstructural and impurity content changes from the as-smelted ingots.
3. A sample of the initially forged blade, after the low and high carbon pieces were forge welded together but prior to heat treatments and hardening, was evaluated to determine any microstructural changes due to the forging process.
4. A sample of the final sword steel, after heat treatments and hardening, could not be extracted since that would damage the blade. Instead an attempt was made to examine the edge itself which showed to be difficult due to the fact that the blade is rather large.
5. A small cross-sectional piece of a 1000-year-old spearhead was evaluated for a historical microstructure and content comparison with the UC Berkeley blade.

3.1.3. Experimental Details

All samples collected were mounted in cold epoxy. The mounted samples were systematically ground with increasingly finer grades of silicon carbide papers (320 → 400 → 600 → 800 → 1200), followed by incremental polishing steps with diamond suspension solutions of decreasing particle size (15μm → 6μm → 3μm →1μm). It was crucial that the samples were finely polished since pristine sample surfaces with minimal scratching are required for EDS and Vickers hardness experimentation as well as chemical etching which was also Nital (3% nitric acid with ethanol) . A high quality polish was confirmed with OM. The polished samples were placed in the SEM to characterize the metal surface and inclusions with EDS. EDS is an analytical surface analysis technique that detects the emitted characteristic X-rays (element-specific) that form as a high-energy electron beam rastered across the sample. The SEM voltage and current were set at 30keV

and 4nA respectively during EDS experimentation. The map and line scan EDS data collection modes enabled local and detailed chemical identification of the inclusions embedded within the high, low, and mixed carbon steel matrices. For EDS map scans, the detected elements are mapped onto the SEM image, i.e. over the selected area of interest. This type of scan was done on regions with varying sized inclusions. A line scan, drawn across an inclusion, was performed to detect any variations in chemical content within an inclusion. EDS was performed on samples both before and after etching to better define the degree of solute segregation.

All of the polished samples were etched with Nital 3%(3% HNO_3) etching solution (The same etchant used for the sword). The etchant was applied to the sample surfaces for approximately ten seconds. Interestingly, low carbon regions required longer etchant exposure time to reveal the grain boundaries and microstructure which might be due to the fewer carbide/Fe interfaces. Multiple OM images, with magnifications ranging from 50X to 500X, of the etched surfaces were recorded and analyzed to estimate each sample's dominant microstructure and carbon content. This was possible since etching affects the microstructure of the various steel phases differently, i.e. different colors and intensities are observed given a specific microstructure. For example, ferrite (α phase) has a body-centered cubic (BCC) crystal structure and appeared light-colored when etched, while Perlite which is a laminar structure between cementite (Fe_3C phase) and ferrite (Fe), appears darker and even brown colored in the optical microscope. Furthermore, pearlite is a layered ferrite/cementite structure, and as expected, exhibited striped pattern after etching. Once the individual microstructures/phases were identified, the overall carbon concentration of the steel was approximated by quantifying the area fraction of each phase in the OM image area and multiplying each phase by its known carbon content. The maximum carbon solubility in ferrite and cementite are known to be ~ 0.02 wt.% C and 6.67 wt.% C respectively as it can be seen in the Fe-C phase diagram of figure 3. The perlite (lamellar appearing structures) is the eutectic microstructure of steel and it is known that it contains 0.8wt% carbon. The microstructural compositions, revealed by etching, were further quantified with additional EDS measurements.

Cementite is harder than ferrite due to its much higher carbon content. The carbon atoms not only alter the atomic structure (BCC vs. orthorhombic) but also cause the structure to become more rigid, i.e. harder, since carbon forms more covalent/directional bonds than iron. The hardness of the samples was measured using the Vickers hardness testing method. The low and high carbon regions of the polished and etched sample surfaces were indented with a diamond Vickers indenter. The applied load was 1 kgf and the diagonal length of the indents was measured in the OM subsequently. Since the plastic zone around the indention site was about four times the size of the indention site itself, i.e. encompassing multiple high and low carbon phases, the Vickers hardness value was more representative of an average hardness for the sample. The local hardness measurements of the individual phases/microstructures were calculated using the same diamond indenter mentioned previously but with an applied load of 0.2 kgf. The following equation was used to calculate hardness value according to the Vickers hardness testing method.

$$HV = \frac{1.8544F}{D^2} \qquad \text{Equation 15}$$

Where F is the applied force in units of [kgf] and D is the diagonal length of the indention profile in units of [mm]. The unit of the Vickers hardness value is known as HV, or the Vickers pyramid

number. Optical microscopy and Vickers hardness testing were also conducted on a portion of the final sword edge to evaluate the final microstructure and the effectiveness of the hardening heat treatments. However, these data are not as of the same quality as the other data collected due to the large blade manufactured which does not fit well in the instruments.

3.2. Experimental results and analysis

3.2.1. Sample of the as refined condition

Figure 13 is an optical micrograph of the as polished condition. The as-smelted ingot contained numerous inclusions distributed over the entire sample. Prior to etching, a clear grain structure was not visible and no OM observations about the microstructural phases were made. However, EDS analysis on the same sample provided details on the inclusion composition.

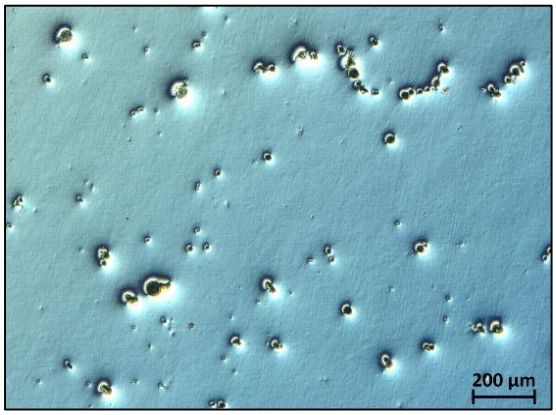

Figure 13: OM image of a polished surface of the as-smelted low carbon ingot at 500X magnification. Not etched

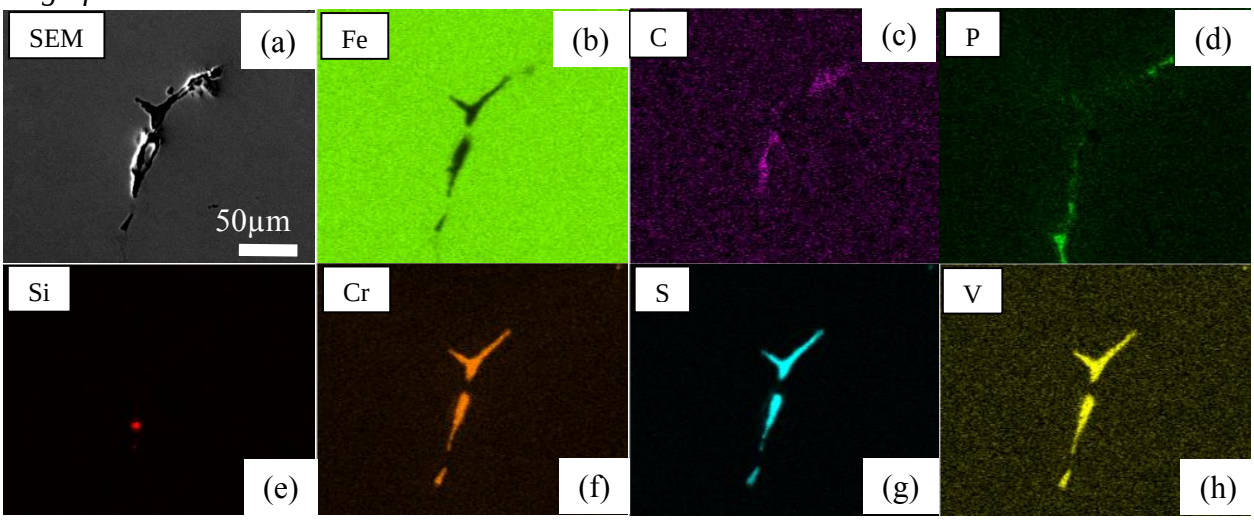

Figure 14: EDS elemental mapping analysis of an inclusion embedded in the as-smelted low carbon ingot; a) SEM image of the inclusion. Elemental distributions of: b) iron (Fe); c) carbon (C); d) phosphorous (P); e) silicon (Si); f) chromium (Cr); g) sulfur (s); and h) vanadium (V).

It can be concluded that the inclusions are non-metallic due to the high P and S content. This is supported by the fact that phosphates and sulfides are common impurities found iron ores. Cr, S and V appear to be confined within the inclusion whereas P and C are more diffuse. This may be related to the solubility of these elements in Fe. The detection of Si could be an inclusion from the manufacturing but also be an artifact of polishing, where polishing SiC particles can be embedded in the surface. However, since no local carbon increase is seen it is likely that it is from the ore and its processing.

Optical micrographs of the samples taken after etching revealed a large grained ferrite + perlite structure. The etchant caused ferrite grains to appear brighter than the perlite grains.

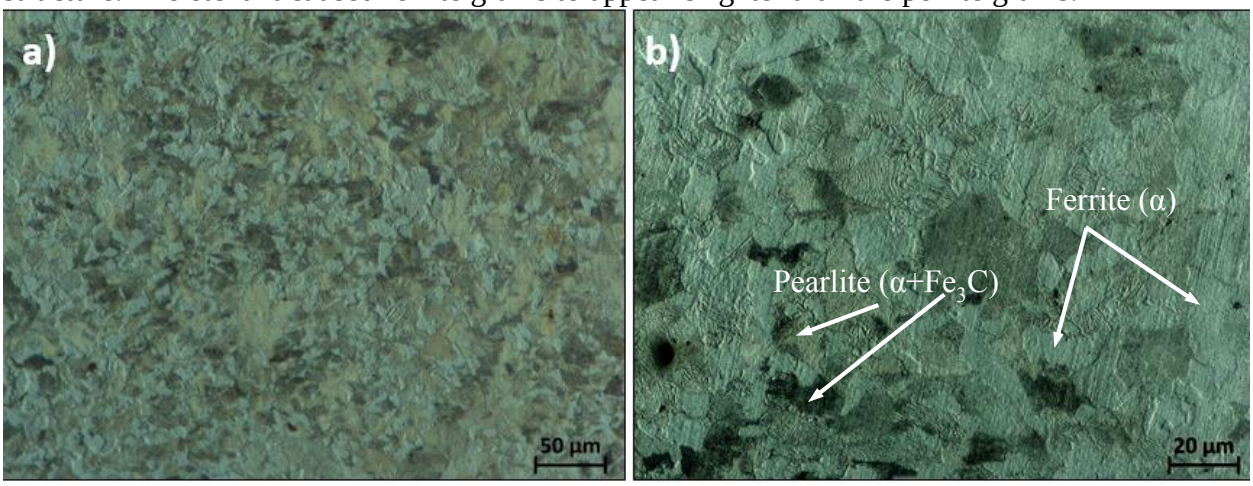

Figure 15: OM images of the as-smelted low carbon ingot's surface after polishing and etching with Nital 3% at a) 200X and b) 500X magnifications

The diagonal measurements of the surface indention profiles from an applied load of 1 kgf were used to calculate the Vickers hardness values by equation 16. It was found that the hardness measured was 230.5HV with a standard deviation of 5.4 over a total of 6 indents.

3.2.2. Sample of the high and low carbon material laminated together by forge welding

As described previously, a spark test was performed to distinguish the manufactured low and high carbon steels from one another [2]. The as-smelted ingots were cut and forged into strips. The low carbon steel strips were forge-welded together into two low carbon packets. The same was done to the high carbon strips, which formed one high carbon packet. The three packets were then stacked, with the high carbon packet in the middle, and forge welded together. Figure 16-a shows an optical micrograph of the low carbon (left) and high carbon (right) interface. Interestingly, the lower carbon side contained more inclusions than the higher carbon side. The low carbon side has been folded 36 times while the high carbon side has been folded 12 times. In addition the low carbon side was longer liquid to allow for higher carbon pickup. EDS was performed on a large inclusion in the low carbon region, see Figure 17. The inclusion was confirmed to be a rather large Cr, Al oxide particle surrounded by a Si, Ti, and Ca casing. The shell was deformed around the oxide inclusion in parallel to the blade length axis. This would indicate that the inclusion comes from the melt and not from the laminating process (surface oxide) since Ca was sued in larger quantities during smelting and a non-metallic Ca containing phase surrounded an oxide phase. Also since the material was deformed around that particle it is likely that it formed prior to the laminating process and therefore is due to the longer heating time of the melt. However, further investigations would be needed in order to confirm this hypothesis.

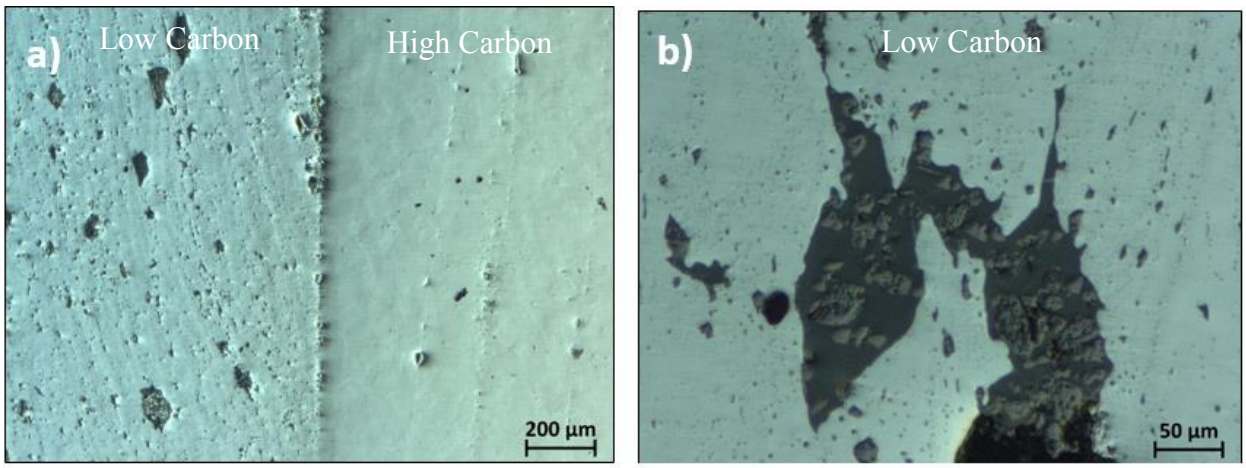

Figure 16: OM images of the forge welded high and low carbon steels. a) 50X magnification. Left side is low carbon region, right side is high carbon region. b) 200X magnification of an inclusion in the low carbon region.

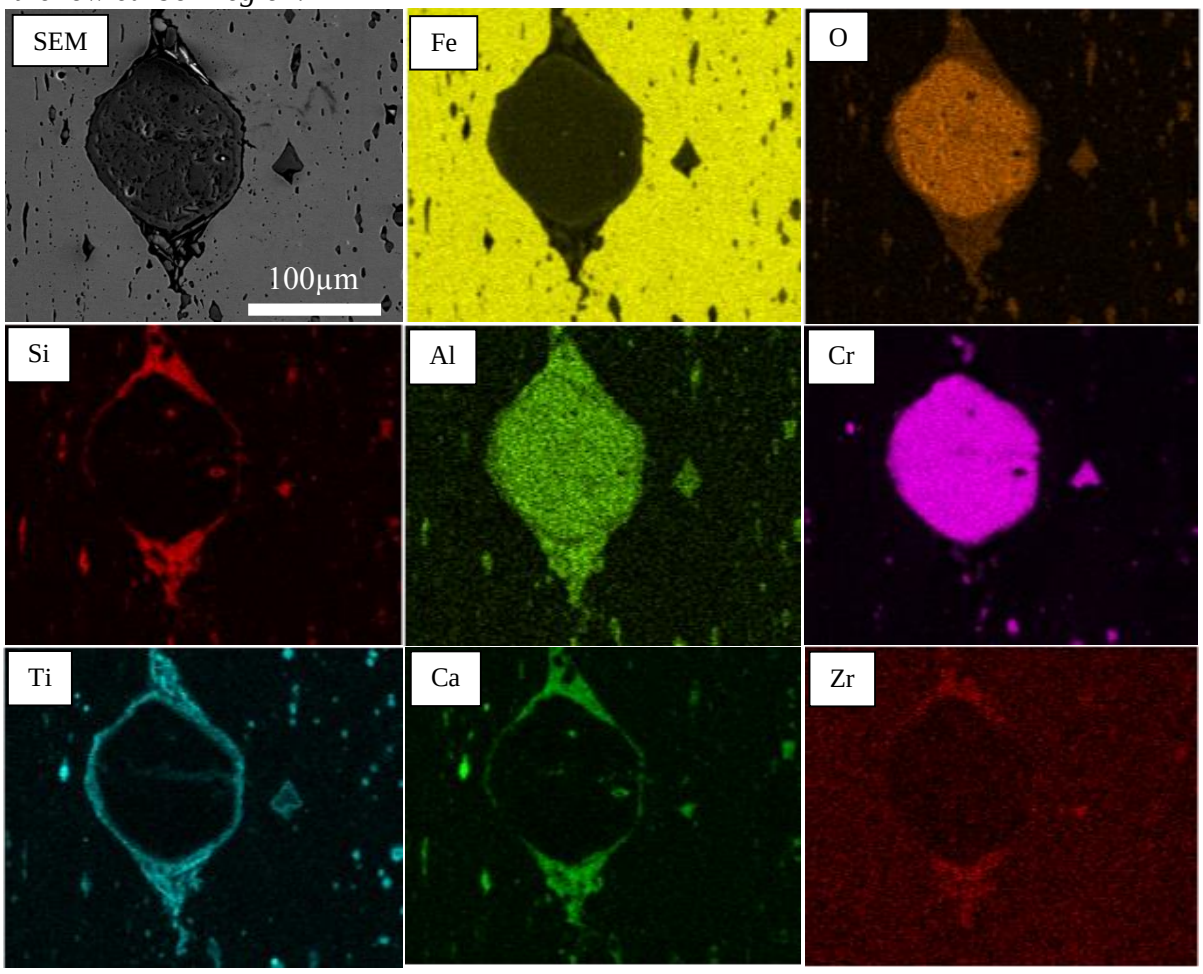

Figure 17: EDS analysis of an inclusion in the low carbon side of the laminated steel. The detected impurity elements were: oxygen (O), silicon (Si), aluminum (Al), chromium (Cr), titanium (Ti), calcium (Ca), and zirconium (Zr). Prior to etching

As before, etching provided enough contrast to observe the phases, and individual microstructures, of the steel. Figures 18 and 19 are the optical and SEM micrographs of the forged high-low carbon after etching. Large inclusions with a strong ferrite perlite microstructure were observed. Interestingly, the low carbon material (outer area) demonstrates signs of higher deformation near the high carbon, center, part of the blade which seems to be plausible since it has been folded more times and since it is softer more work was put into the material.

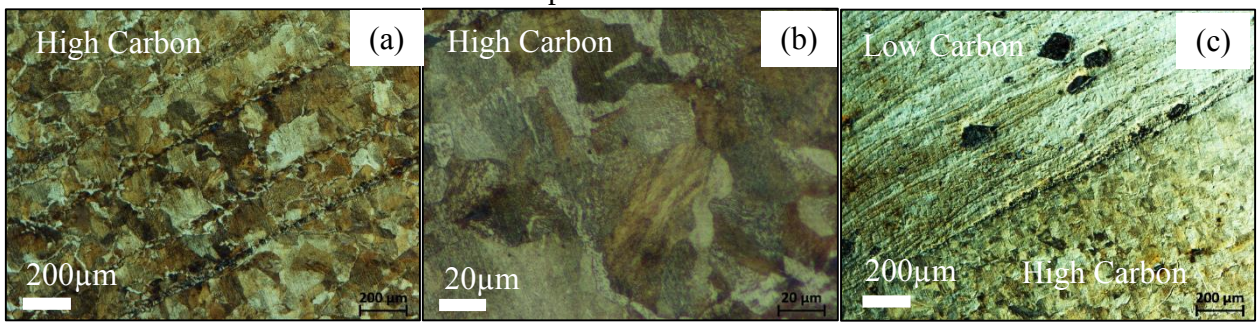

Figure 18: Optical micrographs showing a) high carbon region at 50X and b) 500X, c) interface of low/high carbon at 50X. The brown colored patches are perlite while the white areas are ferrite.

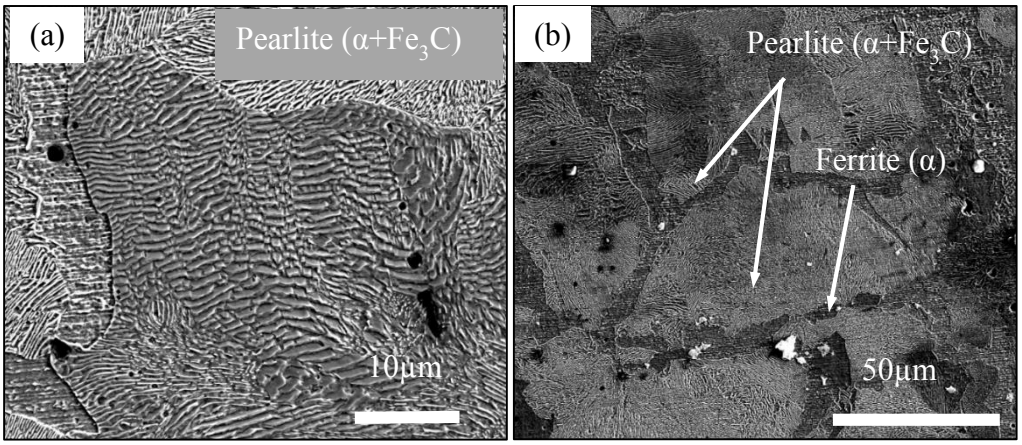

Figure 19: SEM images of high carbon region after etching a) showing perlite structures and b) pearlite and ferrite structures

As predicted, a distinct difference in carbon content between the pearlite and ferrite regions were observed with EDS. Furthermore, the carbon content is highest at the pearlite-ferrite boundaries. This is likely due to the fact that carbon, like most light elements, diffuses to microstructural boundaries and form a line of carbide at the interface.

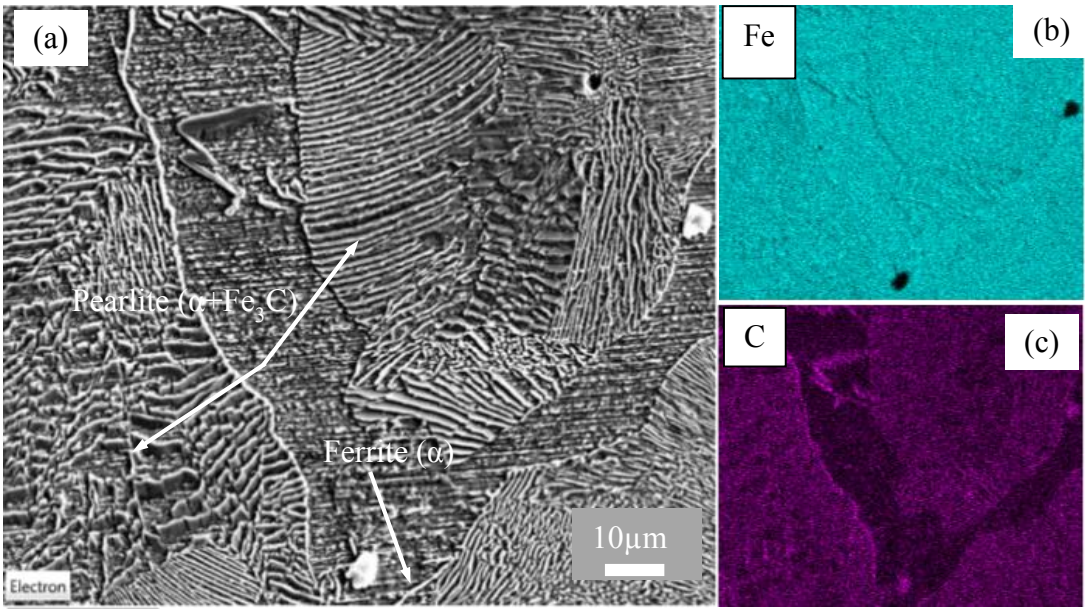

Figure 20: EDS Analysis of a high carbon region. EDS shows a distinct difference in carbon content between ferrite and pearlite regions.

10 hardness indents were made in the low and high carbon region. It was found that the low carbon region has a Vickers hardness of 138.3HV with a standard deviation of 16.3 and the high carbon region had a hardness of 210HV with a standard deviation of 31.

High carbon region forms ferrite pearlite structure, which has higher hardness than the low carbon region, which is mainly made up of ferrite. Interesting to note is that hardness measurement of high carbon region has higher standard deviation which could be due to the fact that less deformation was put into this region and therefore the material being more inhomogeneous.

3.2.3. Sample of the material after blade was formed and prior to hardening

Figure 21 shows the inclusions in an optical micrograph after the blade was further thinned to its final shape. Again, the interface of the high carbon and low carbon piece can be seen in Figure 22 a while b shows the low carbon side. EDS was conducted on the as final forged material as displayed in Figure 23.

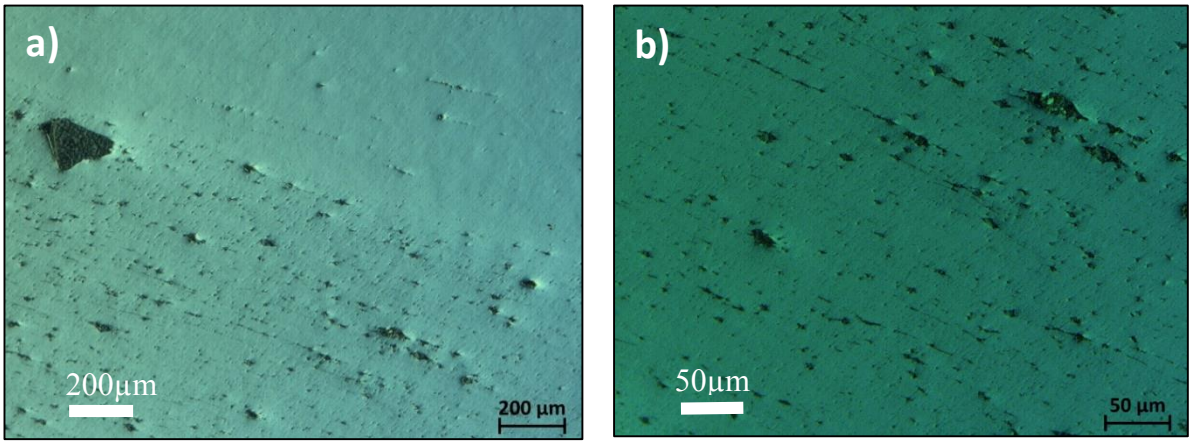

Figure 21: Optical microscope images of the surface (a) high carbon region and low carbon region at 50x (b) low carbon region at 200x

The EDS shows a large numbers of now finer inclusions. The inclusions are in parallel to the blade length axis as expected after forging. Again, Aluminum Titanium inclusions are found. Silicon, Vanadium, Calcium are also observed. Figure 22 shows the optical micrographs after etching.

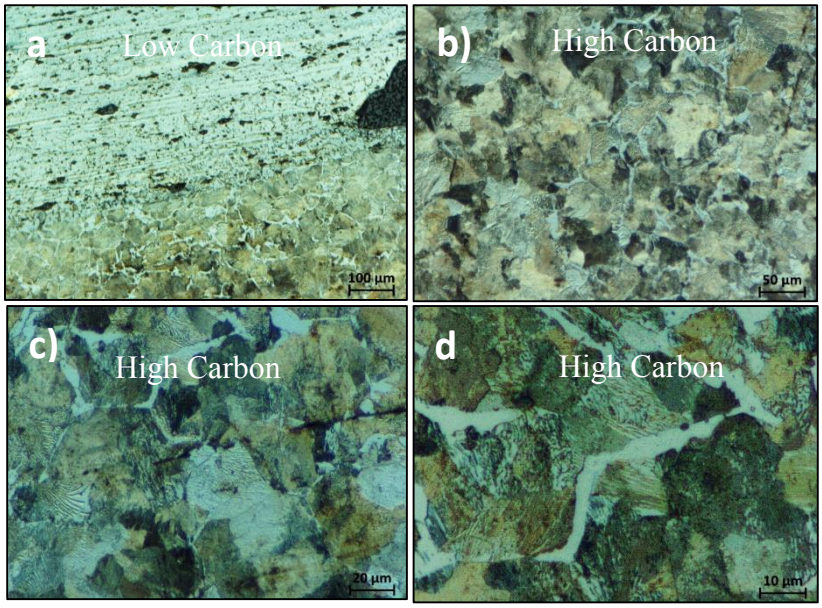

Figure 22: Optical Microscope images of (a) the two regions at 100x (b) high carbon at 200x (c) 500x (d) 1000x

Digital image analysis is done on optical micrographs after etching in order to determine the carbon content of each region as showed in Figure 23. There it can be seen that a grayscale filter was applied to the grain structure outlining the bright (ferrite) and dark (perlite) regions using the image processing tool image J. It was found that this method did miss identified small regions where the spacing between perlite lamellas was larger and more ferritic regions were visible. However, it was also found that this error is rather small comparing figure 23 a and figure 23b and might be neglectable.

Figure 25 and 26 show SEM/EDS micrographs after etching. Again, pearlite and ferrite structures are found. The EDS mapping of the carbon content nicely traces boundary between ferrite and pearlite structures. Figure 26 also shows that ferrite has less iron content than then perlite does. It is also worth noting that the non metallic inclusions are now in a line shape and aligned to each other indicating a large amount of deformation.

Again Vickers hardness measurements were performed on the samples. It was found that the lower carbon region has a hardness of 140HV with a standard deviation of 9. The Vickers hardness number on the higher carbon material was 188HV with a standard deviation of 24. Again it is noted that the standard deviation was higher in the high carbon region.

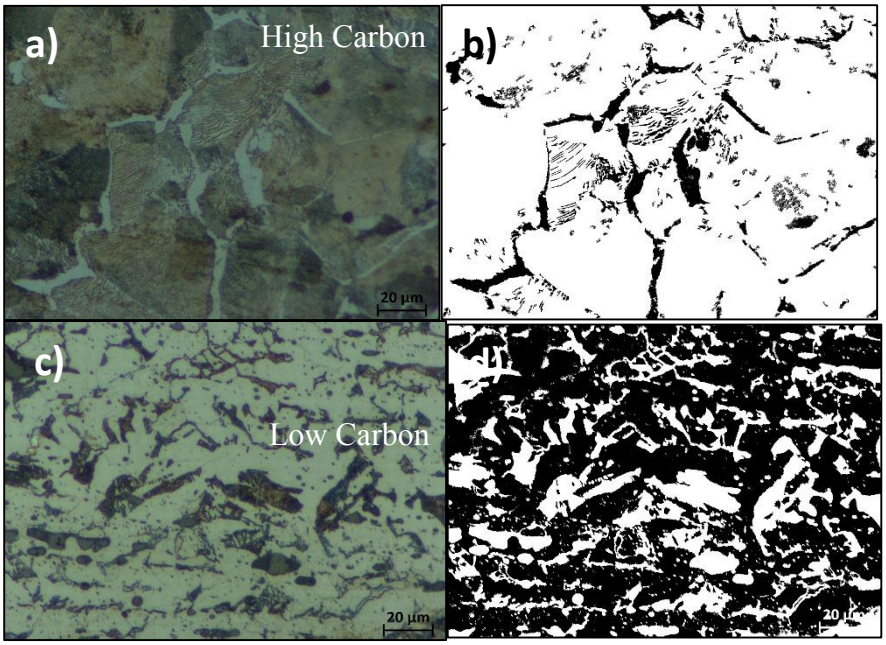

Figure 23: Image analysis for determining carbon content of (a) high carbon region and (b) low carbon region. (c) and (d) are processed images. Total carbon of high carbon region and high carbon region are 0.7% and 0.26% respectively.

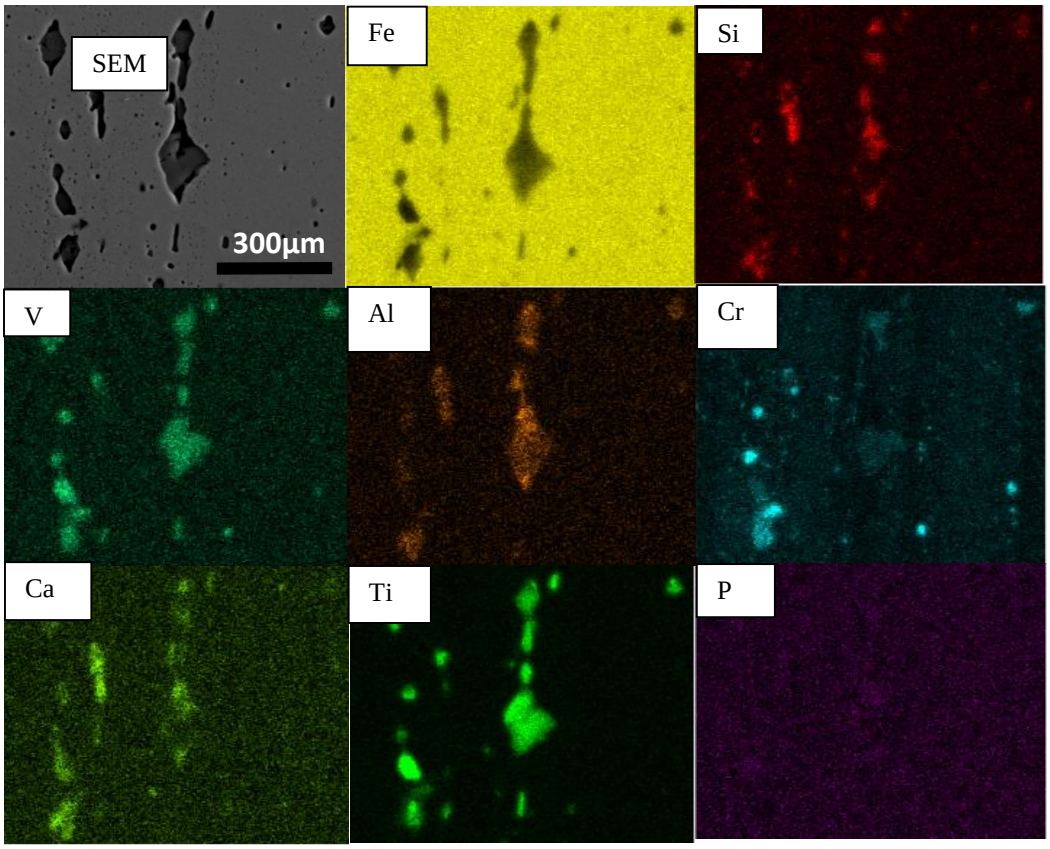

Figure 24: EDS analysis of inclusion region, showing Silicon, Vanadium, Chromium, Titanium and other compounds.

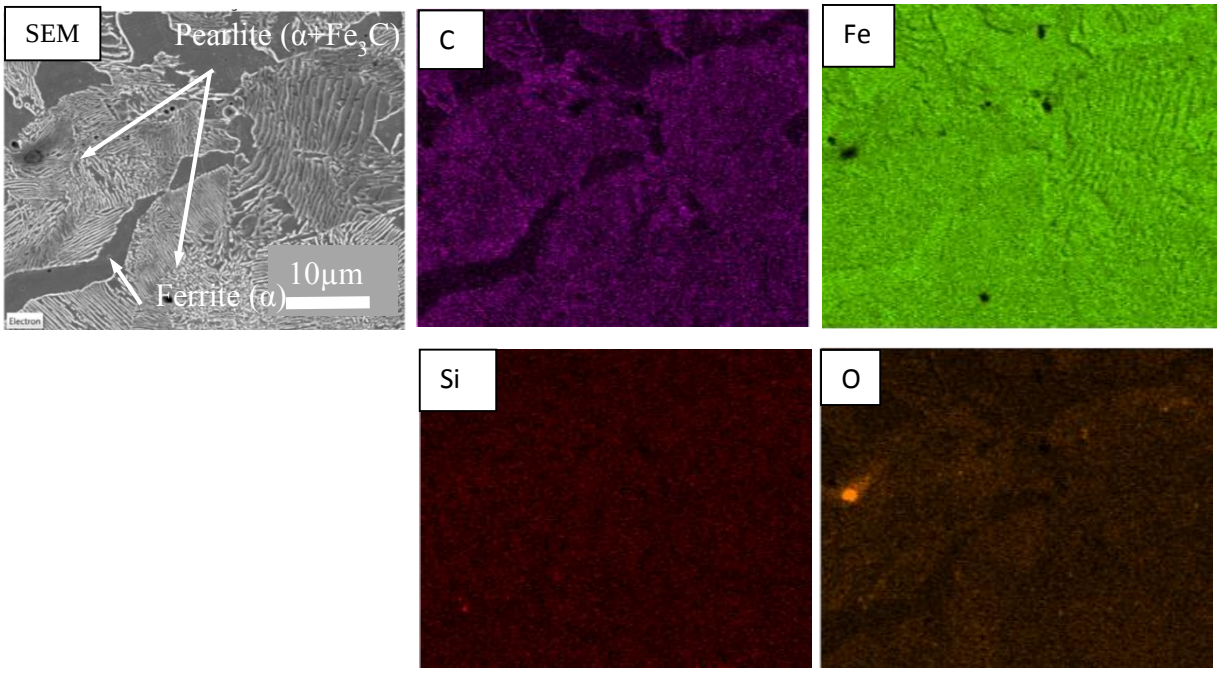

Figure 25: EDS analysis of the high carbon region after etching. The analysis shows a distinct difference in the carbon content between pearlite and ferrite structures.

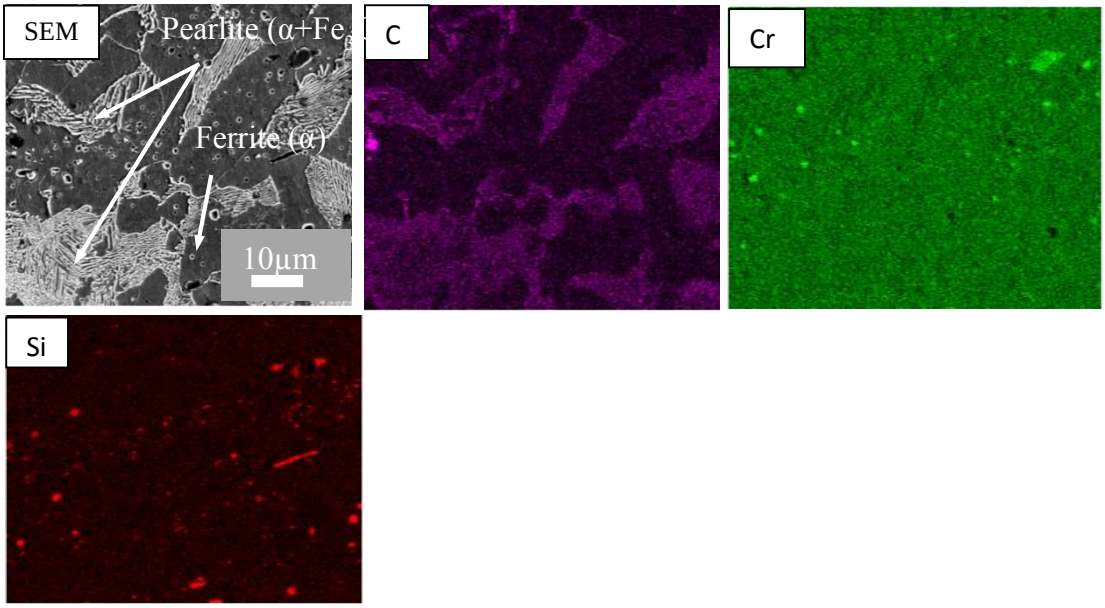

Figure 26: EDS analysis of the low carbon region after etching. The region consists of ferrite and pearlite structures. The analysis shows a difference in carbon content between those structures.

3.2.4. Sample from a 1000 years old spear head

A sample from the collection of the artesian member was prepared in the same fashioning than the other samples of the Berkeley team made material. The sample was originally obtained in an auction and is part of Mr. Austins and his colleague Jeff Pringle's collection. A crises sectional analysis was performed on this diamond shaped specimen. OM images of the as polished condition can be seen in figure 27. Interestingly it was found that the steel is actually surrounded by a layer of another material as it can be seen in figure 27b. Also the sample contains significantly less inclusion than the material made by the Berkeley team. EDS reveals that some amount of Ag is present on the steel as well.

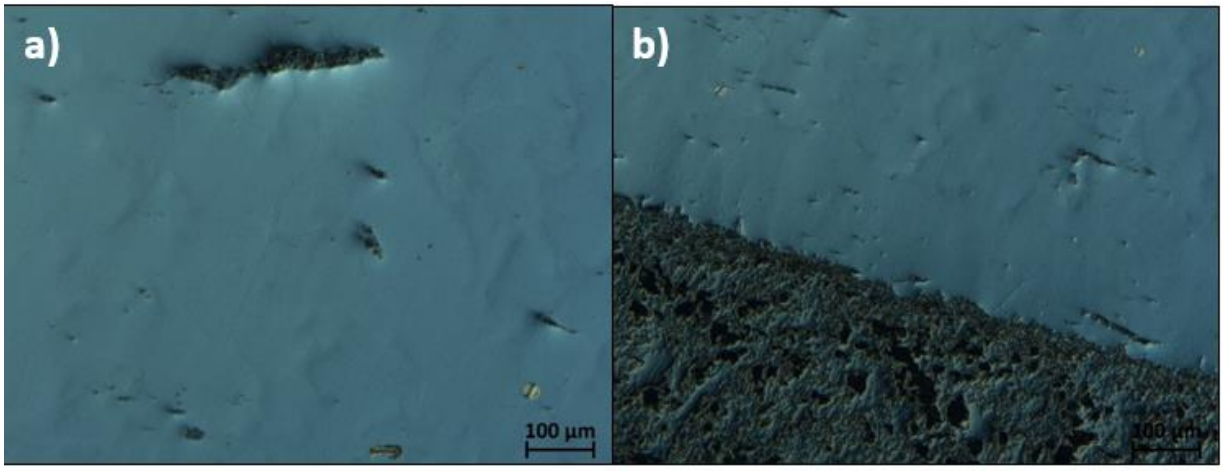

Figure 27: Optical micrographs of (a) the inner region at 100x (b) the coating and the inner region at 100x

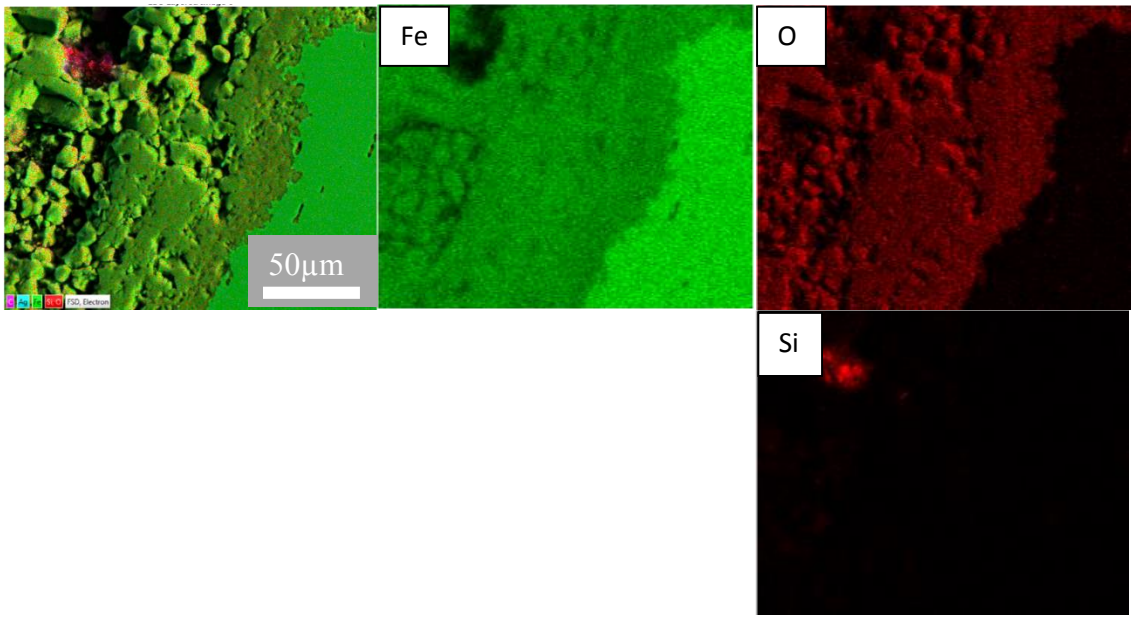

Figure 28: EDS analysis of the coating of the spear, showing Gold, Silicon and carbon compounds

It can be seen that the layer surrounding the metal is Fe-oxide which is most likely caused by the fact that it is an old material and therefore exposed to air and potentially moisture for a long period of time. In addition, several large inclusions are found, as seen in Figure 29. The figure shows EDS

analysis of the inclusion. The left haft of the inclusion contains calcium, aluminum, silicon, manganese, and potassium oxides. The other half contains mainly iron oxide and small regions of calcium, silicon, and potassium. The region also contains Fe and Silver.

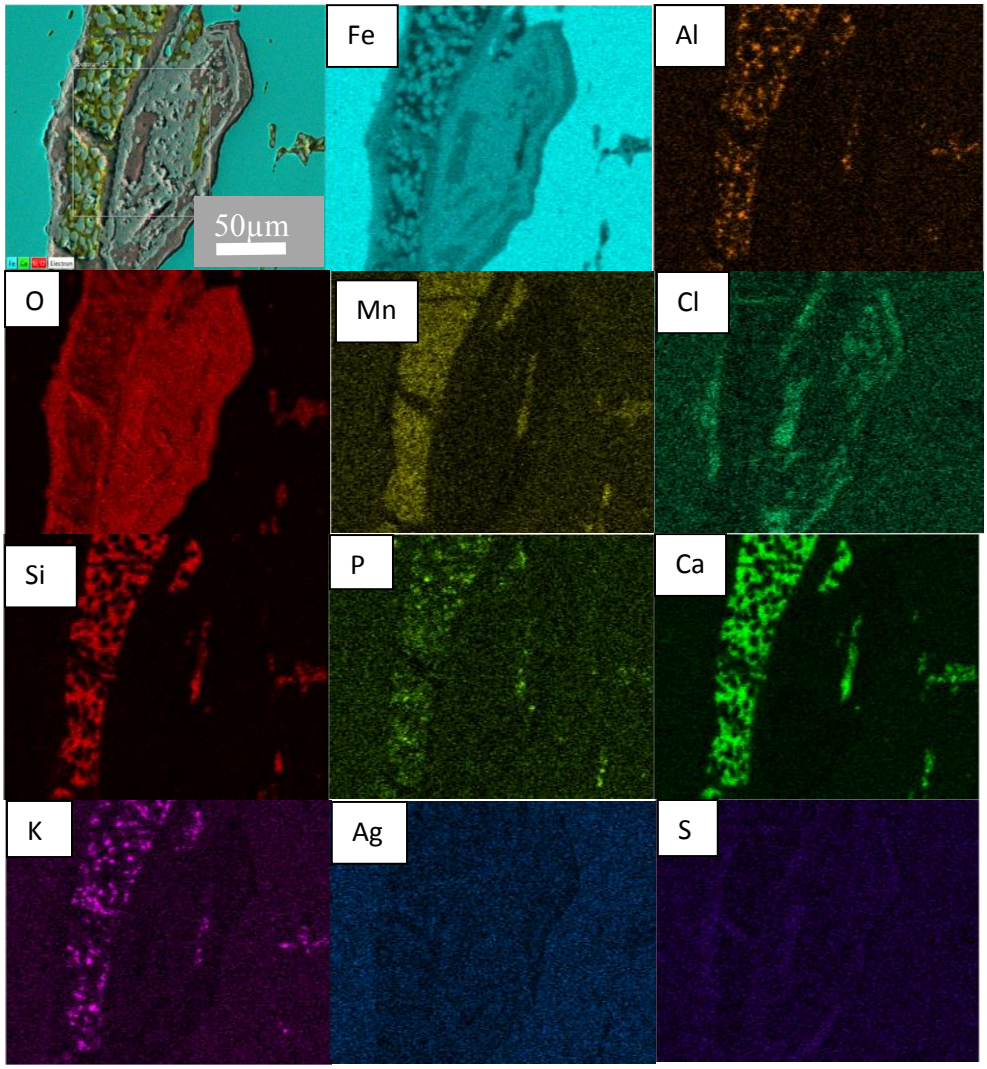

Figure 29: EDS analysis of an inclusion, showing Aluminum, Silicon, Potassium, Manganese and other oxides

Optical micrographs after etching are shown in Figure 30. Again, a ferrite/pearlite structure is found. The ferrite content is much greater than pearlite. Image analysis of topical micrograph shows the total carbon content to be 0.09%, Figure 31. The hardness measured on this sample was found to be 124HV with a standard deviation of 30.

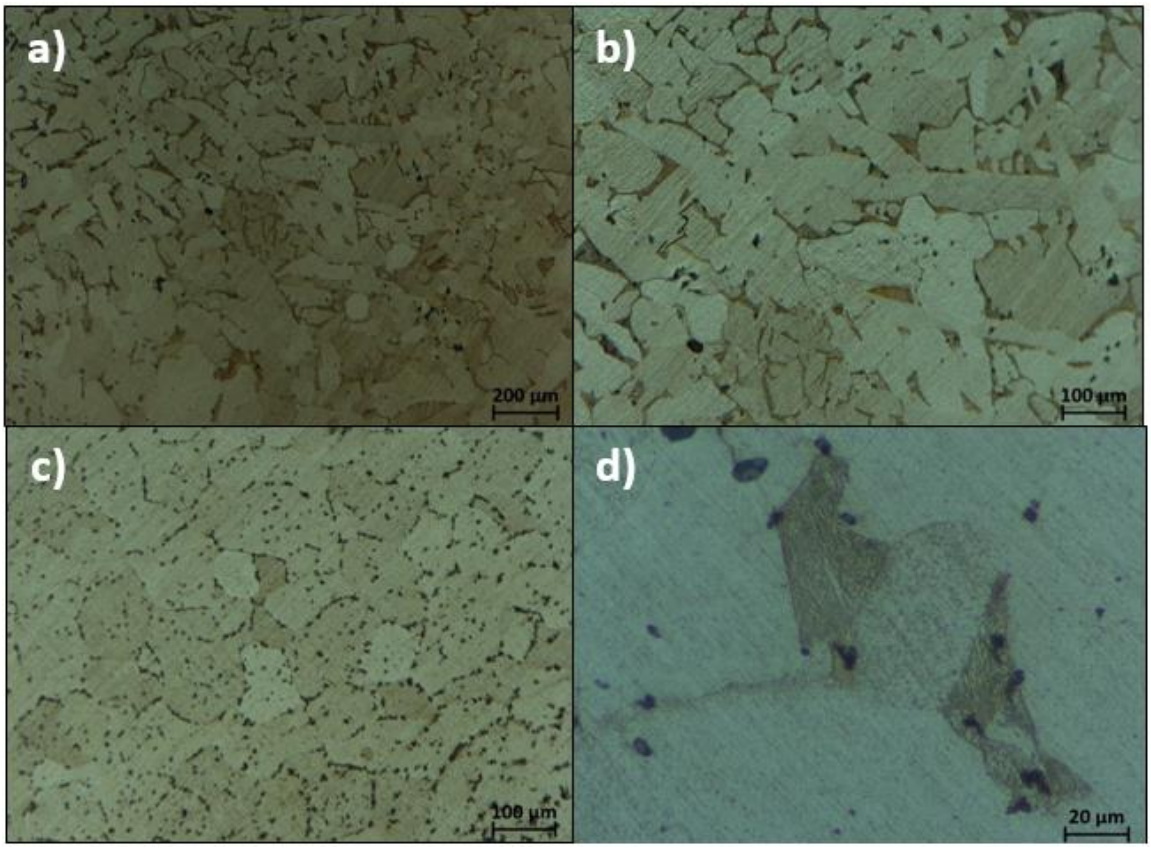

Figure 30: Optical Microscope of the spear sample after etching at (a) 50x (b) 100x (c) 100x (d) 500x.

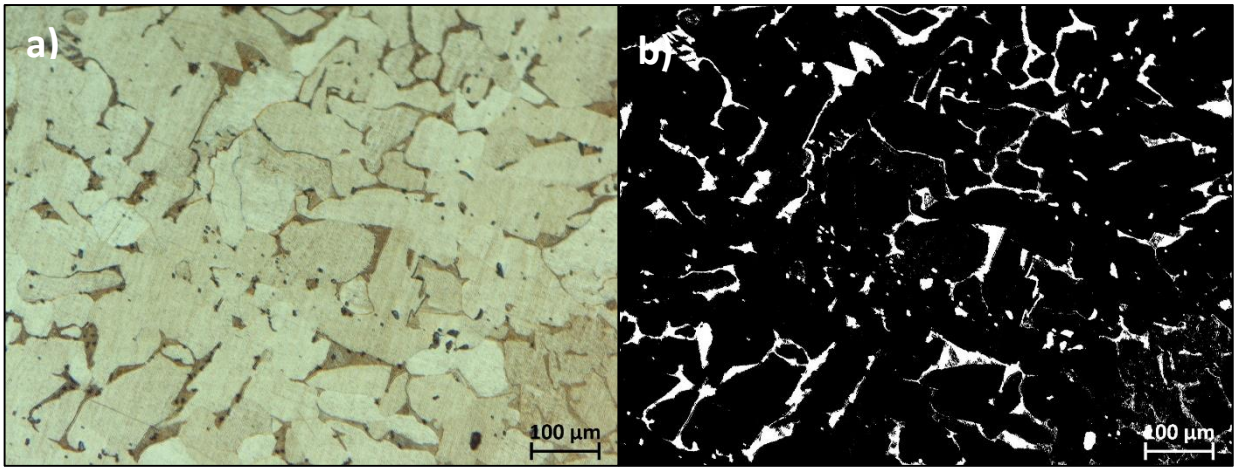

Figure 31: Image analysis for determining carbon content of the spear head showing (a) optical micrograph and (b) processed image. Total carbon = 0.09%

3.2.5. Blade after hardening

As mentioned above an attempt was made to obtain micrographs and hardness values of the actual edge of the blade itself. This however, was found to be rather challenging due to the size of the blade and only low quality images were possible to obtain. In addition the fact that two different materials are joined together made the etching difficult since they etch at different rates. The images displayed in figure 32 show the edge of the blade after etching. The three layers (low carbon and high carbon) can be seen clearly. Needle (lath)-like structure which is indicative for martensite which is difficult to observe. However, this seems to be the case because of the low quality images taken in figure d and the more difficult etching condition. One can maybe see something which could be interpreted as a needle like structure in figure 32 d.

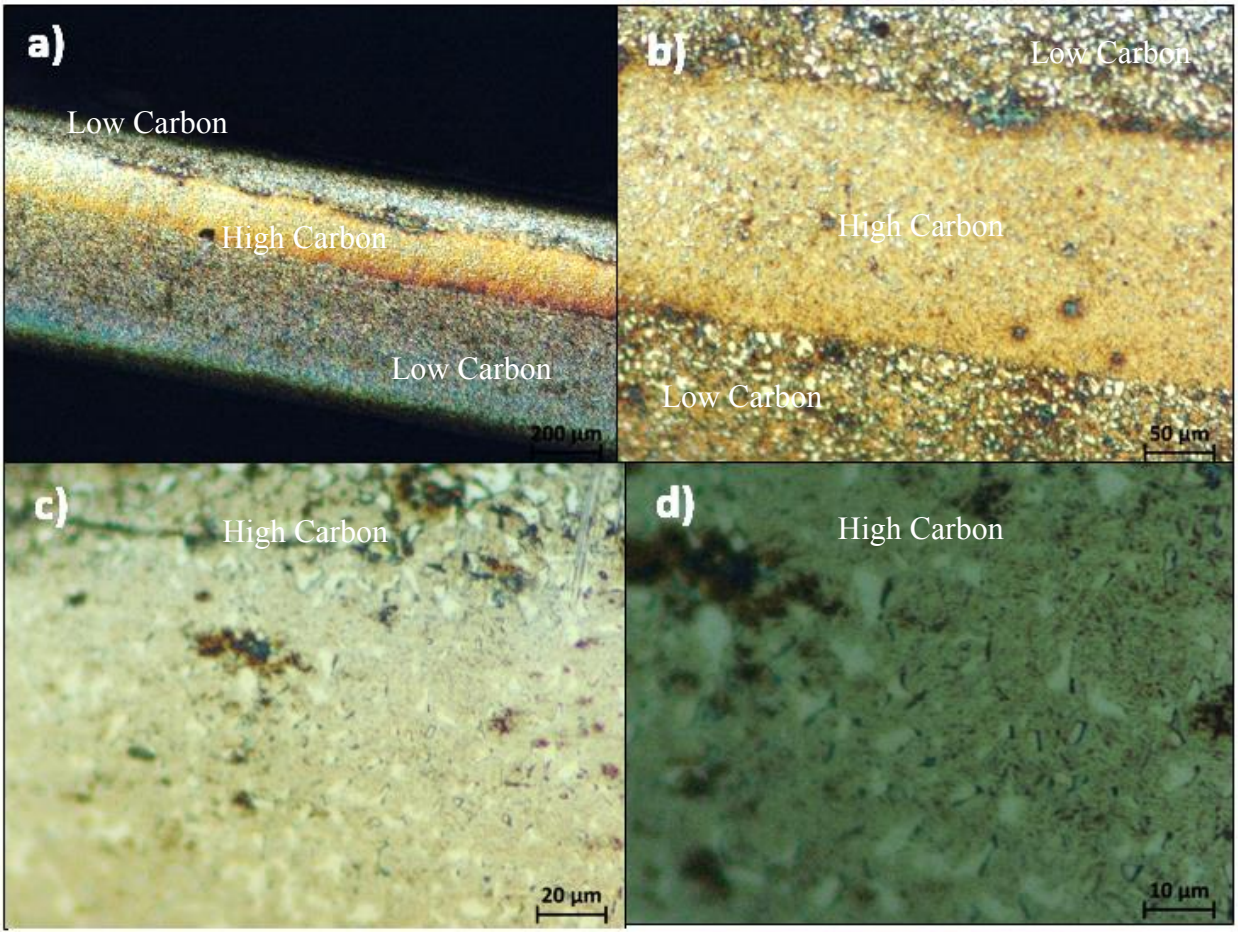

Figure 32: Optical micrographs of the edge of the blade after etching at (a) 50x (b) 100x (c) 100x (d) 500x.

The hardness measurements also confirmed that the heat treatment did significantly increase hardness 467HV in the low carbon region and 699HV in the high carbon region clearly showing the effect of the heat treatment and formation of martensite.

4. Discussion/summary

The material analysis looks at four stages in the manufacturing process. Unfortunately not all stages and samples from each ingot and billet could be analyzed since this would go too far in the time given to finish this project. However, the data obtained is sufficient to get a good understanding of the microstructure and property of the blade manufactured. The characteristics of the homemade material and the historical artifact are compared to each other in order to understand the differences. The homemade materials consist of high carbon and low carbon steels in order to provide ductility and strength making the blade a composite or maybe even a functional graded composite. The spear head is made of low carbon steel only while heavy oxidation is found. The digital image analysis allows to estimate the amount of carbon present in the steel. It is known that perlite contains 0.8% carbon while ferrite contains 0.02% carbon. Using the lever rule we can calculate that that the carbon content of the spear head is 0.09wt% percent while the carbon content of the homemade steel, 0.7wt% percent in high carbon steel and 0.27 %wt percent in low carbon steel, and therefore significant higher than the carbon content in the historical artifact.
We do want to mention that this higher carbon content improves the strength of the blade which can be seen on the hardness numbers reported. Detailed grain size analysis was not performed but it can be seen that the grain size is larger in the spear head than in the homemade steel. It is also worth noting that the spearhead has sign cant less nonmetallic inclusions than the material produced here.

The low carbon steel specifically contains many inclusions of various compounds. EDS analysis shows that chromium aluminum particles with titanium calcium shell are found. The high carbon steel contains much less inclusions. A large particle made of silicon, manganese, calcium, and other oxides is found in the sample.

Before heat treatment a ferrite pearlite structure is found in both samples after quenching, formation of martensite is found on the blade edge. The grain size, carbon content, and microstructure contribute to the difference in hardness values of the samples. The microhardness of the spear sample, 125 HV, is lower than the blade's micro hardness, 141 HV in low carbon region and 288 HV in high carbon region. After hardening, the average hardness of the blade edge is 699 HV in high carbon region and 467 HV in the low carbon region. Because the hardening effect is not homogenous throughout the blade edge, the micro hardness value varies greatly in different regions. Evaluating the literature it was found that our hardness values fall within the hardness expected after heat treatment. In [6] it was found that the hardness after quenching and annealing a hardness of ~700HV is found on a 0.7wt%C steel while a hardness of ~450HV is found after the same treatment on a 0.27wt%C steel. These numbers agree rather well with our measurements found here as indicated in Figure 33. Also comparing the microstructure in [6] to the microstructure here similarities can be found. The antique spear head cannot be compared since it was not heat treated (no martensite found) which indicates that this spear was not used but more a decorative piece since it is too soft.

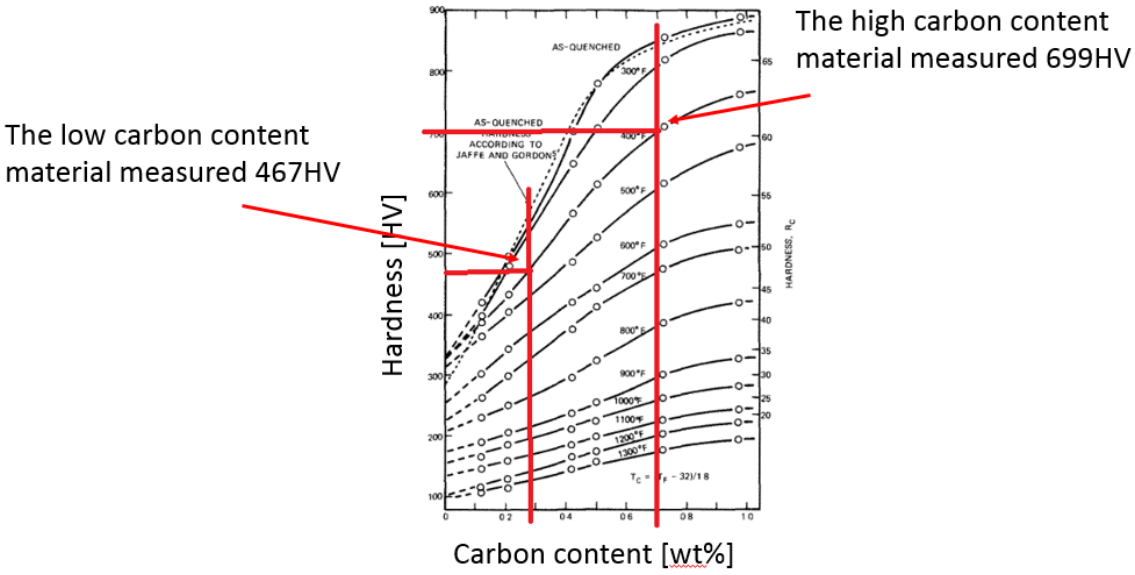

Figure 33: Data comparison with the literature. The red lines indicate the carbon content of the materials investigated here and the resulting hardness. [6]

5. Conclusion

This was a successful sword-making project. Following the guidance of our expert advisor we are able to present a completely in house manufactured blade. In addition we were successful in creating a laminated and functional graded material with a higher hardness in the middle (cutting edge) and a softer body which will allow to hold a good edge if the blade is sharpened while it won't shatter while it is struck with another hard object. The large number of large inclusions in the home made material are unfortunate but were unavoidable during the process. There is potential for improving the process by producing higher carbon material since there appears to be less inclusions in the higher carbon part of the blade. One can then further decarburize the material after the smelting process.

However, the fact that our team was able to manufacture steel and a blade from magnetite containing sand collected in nature is a true achievement and the team benefited from this project tremendously and was an exciting experience.

The blade shape was modeled after a Viking saex. This was done both to simplify the blade shape in order to reduce the risk of catastrophic mistakes during the hand forging process, as well as to showcase the innate beauty of the layered steel we used. For future projects, more complex blade designs such as double edged blades could be made.

6. References

[1] Patrick L. Barnard et al:" Integration of bed characteristics, geochemical tracers, current measureme0nts, and numerical modeling for assessing the provenance of beach sand in the San Francisco Bay Coastal System " marine Geology 336 (2013) 120-145
[2] H. Schumann, H. Oettel Metallogrpahy, Wiley-VCH 2005 ISBN 3-527-30679
[3] R.W. Buzzard; The utility of the spark test as applied to commercial steel. U.S. Department of Commerce Bureau of Standards Vol 11 (1933)527-540
[4] Oberg, Erik; Jones, Franklin Day (1918), Iron and Steel (1st ed.), The Industrial Press.
[5] W. Rasband ImageJ 1.48V
[6] R. A. Grange, C. R. Hribal, L. F. Porter; Hardness of tempered martensite in carbon and low-alloy steels; Metallurgical Transactions A; 8 (1977) 1775-1785